Magnetic Excitations of the Classical Spin Liquid $MgCr_2O_4$

X. Bai,[1] J. A. M. Paddison,[1,2] E. Kapit,[3,4] S. M. Koohpayeh,[5] J.-J. Wen,[5,*] S. E. Dutton,[6,†] A. T. Savici,[7] A. I. Kolesnikov,[7] G. E. Granroth,[7] C. L. Broholm,[5,7] J. T. Chalker,[3] and M. Mourigal[1,5,‡]

[1]*School of Physics, Georgia Institute of Technology, Atlanta, Georgia 30332, USA*
[2]*Churchill College, University of Cambridge, Storey's Way, Cambridge CB3 0DS, United Kingdom*
[3]*Rudolf Peierls Centre for Theoretical Physics, University of Oxford, Parks Road, Oxford OX1 3NP, United Kingdom*
[4]*Department of Physics, Colorado School of Mines, Golden, Colorado 80401, USA*
[5]*Institute for Quantum Matter and Department of Physics and Astronomy, The Johns Hopkins University, Baltimore, Maryland 21218, USA*
[6]*Department of Chemistry, Princeton University, Princeton, New Jersey 08544, USA*
[7]*Neutron Scattering Division, Oak Ridge National Laboratory, Oak Ridge, Tennessee 37831, USA*

(Received 28 October 2018; published 5 March 2019)

We report a comprehensive inelastic neutron-scattering study of the frustrated pyrochlore antiferromagnet $MgCr_2O_4$ in its cooperative paramagnetic regime. Theoretical modeling yields a microscopic Heisenberg model with exchange interactions up to third-nearest neighbors, which quantitatively explains all of the details of the dynamic magnetic response. Our work demonstrates that the magnetic excitations in paramagnetic $MgCr_2O_4$ are faithfully represented in the entire Brillouin zone by a theory of magnons propagating in a highly correlated paramagnetic background. Our results also suggest that $MgCr_2O_4$ is proximate to a spiral spin-liquid phase distinct from the Coulomb phase, which has implications for the magnetostructural phase transition in $MgCr_2O_4$.

DOI: 10.1103/PhysRevLett.122.097201

The classical pyrochlore Heisenberg antiferromagnet is a canonical model of frustrated magnetism. With only nearest-neighbor (NN) exchange interactions, it does not exhibit magnetic ordering down to zero temperature, and instead, it hosts a liquidlike state of strongly correlated spins. In real space, this cooperative paramagnet is a system of underconstrained spins on a network of corner-sharing tetrahedra. The energy is minimized if the vector sum of spins is zero on every tetrahedron, giving rise to an extensive ground-state degeneracy. Mapping spin variables to flux variables on the bonds of the dual diamond lattice transforms this spin constraint to a divergence-free condition on the flux fields. Consequently, spin correlations decay algebraically in real space, and sharp features—known as pinch points—are present in reciprocal space. This exotic magnetic state of matter is termed a Coulomb phase [1–5].

The best candidate materials to realize the Coulomb phase include spin ices [6–8], the cubic AB_2O_4 spinels, and $NaA'B_2F_7$ fluorides [9–11], in which a transition-metal ion B occupies a pyrochlore lattice. Canonical spinel examples are $CdCr_2O_4$ [12], $ZnCr_2O_4$ [13], and $MgCr_2O_4$ [14,15], which are all highly frustrated antiferromagnets that ultimately order magnetically at temperatures T_N much smaller than the scale of exchange interactions. Contrary to expectations, neutron-scattering experiments on these spinels do not reveal sharp pinch points; instead, only broad ringlike diffuse scattering patterns are observed. These experimental observations have been explained in terms of decoupled hexagonal spin clusters—loops of six spins with alternating directions [16]. While this phenomenological model has been remarkably successful in explaining magnetic scattering features [13–15,17], it leaves three key questions unaddressed. First, what is the microscopic origin of clusterlike scattering in terms of the underlying magnetic interactions? Second, how does frustration relate to the complex ordered structures that B-site spinels often exhibit below T_N? And, third, what is the origin of the broad magnetic excitation spectrum observed in the cooperative paramagnetic state? This final question is of particular importance because three explanations have been proposed: (i) scattering is broad in energy because excitations have a short lifetime, (ii) scattering is broad because the excitations are fractionalized, and (iii) scattering is broad in momentum because the excitations are riding on a disordered background.

In this Letter, we use a combination of neutron spectroscopy and modeling to determine the spin Hamiltonian of $MgCr_2O_4$ and the nature of its magnetic excitations in the correlated paramagnetic regime at temperature $T = 20$ K. We study this material because it is a paradigmatic example of a frustrated antiferromagnetic spinel that shows clusterlike scattering above T_N and exotic magnetic order below T_N. Our results significantly advance previous studies by measuring and explaining the entire four-dimensional (4D) magnetic response of $MgCr_2O_4$ as a function of energy and momentum. We use quantitative modeling to determine a set of exchange interactions that

best reproduces our experimental data. Remarkably, we find that linear spin-wave theory accurately captures all the details of the correlated paramagnetic response in $MgCr_2O_4$, revealing the harmonic nature of excitations in this classical spin liquid. Furthermore, we find that our model remains highly frustrated despite the presence of further-neighbor (FN) interactions. We explain this result by showing that $MgCr_2O_4$ is proximate to a highly degenerate spiral-spin-liquid phase distinct from the Coulomb phase. Our results suggest that competition between nearly-degenerate states drives the complex low-temperature states often observed in frustrated B-site spinels.

The crystal structure of $MgCr_2O_4$ at $T = 20$ K is cubic (space group $Fd\bar{3}m$, $a = 8.33$ Å). Magnetic Cr^{3+} ions interact magnetically with their nearest neighbors (NN) primarily via direct exchange ($d_{\mathrm{Cr-Cr}} = 2.95$ Å) and with further neighbors (FN) via superexchange [Fig. 1(a)]. Thermomagnetic measurements [18–21] reveal net antiferromagnetic interactions with a Weiss constant ranging from $\theta_W = -346$ K [18,19] to -433 K [20,21], and they are compatible with spin-only magnetic moments for Cr^{3+} ($S = 3/2$ and $g \approx 2.05$) [20]. Below $\sim$40 K ($\approx 0.1\theta_W$), the magnetic susceptibility markedly departs from the Curie-Weiss law, in contrast with predictions for the NN model [22]. Furthermore, a cooperative paramagnetic regime appears with clusterlike scattering [14,15,17,23]. This regime persists down to $T_N \approx 13$ K [20,21,24], where the onset of long-range magnetic ordering [18,20,21] is accompanied by a structural distortion to tetragonal or lower symmetry [25–27] due to spin-lattice coupling [13,16,28,29]. Magnetic Bragg peaks observed below T_N are indexed by two inequivalent propagation vectors, $\boldsymbol{k}_{L,1} = (\frac{1}{2}, \frac{1}{2}, 0)$ and $\boldsymbol{k}_{L,2} = (1, 0, \frac{1}{2})$ [30] with respect to the cubic cell; the magnetic structure of this so-called "L phase" is not fully solved [23,30]. Moreover, an additional partially-ordered magnetic phase ("H phase") with a single propagation vector $\boldsymbol{k}_H = (0, 0, 1)$ is observed for some samples between T_N and $T_H \approx 16$ K [14,30].

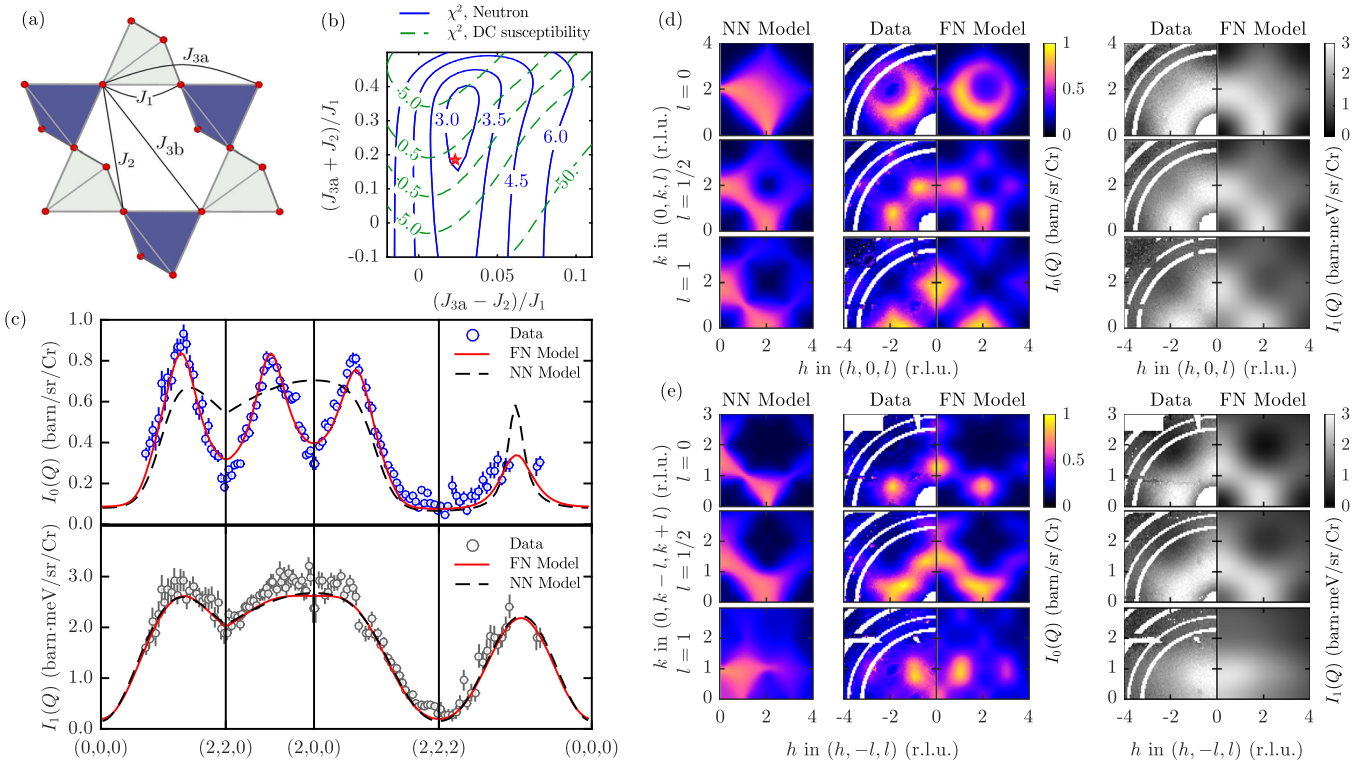

FIG. 1. (a) The pyrochlore lattice of Cr^{3+} ions (red spheres) in $MgCr_2O_4$ and definition of exchange interactions up to third neighbors. Note that J_{3a} and J_{3b} span the same distance but are not equivalent by symmetry. (b) Contour plot of the goodness of fit χ^2 between calculations and neutron (blue solid lines) and bulk susceptibility (green dashed lines) measurements. FN exchange interactions J_2 and J_{3a} are fixed on a grid with J_1 and J_{3b} fitted at each grid point. The choice of $J_2 \pm J_{3a}$ as plotting axes highlights the nearly equivalent spin structure factors obtained for $J_2 = J_{3a}$. Spin correlations are calculated using the self-consistent Gaussian approximation (SCGA) at $T = 20$ K. The red star is the best overall fit. (c) Momentum dependence of $I_0(\mathbf{Q}) = F(|\mathbf{Q}|)\mathcal{S}(\mathbf{Q})$ and $I_1(\mathbf{Q}) = F(|\mathbf{Q}|)\mathcal{K}(\mathbf{Q})$ along several paths of the Brillouin zone (BZ) at $T = 20$ K, and comparisons with SCGA predictions for NN (dashed black line) and FN (solid red line) models. For the NN model, $J_1 = 38$ K. (d)–(e) Selected reciprocal-space planes showing $I_0(\mathbf{Q})$ and $I_1(\mathbf{Q})$, as labeled in the figure, and comparison between NN and FN models calculated using the SCGA. Throughout, white rings are masked aluminum background lines. In (c)–(e), only $E_i = 80$ meV data are shown, but both 40 meV and 80 meV data were included in fits.

To understand the nature of the magnetic excitations in $MgCr_2O_4$ we performed neutron-scattering experiments that expose its magnetic excitation spectrum as a function of neutron momentum transfer $\hbar\mathbf{Q} = \hbar\mathbf{k}_i - \hbar\mathbf{k}_f$ and energy transfer $E = E_i - E_f$ to the sample. Large single crystals of $MgCr_2O_4$ were grown using the floating-zone technique following systematic sample-quality studies [20,21]. Our 10 best crystals were coaligned on an aluminum holder for a total sample mass $m \approx 13.5$ g and overall mosaic $\leq 3°$ (see Supplemental Material [31], Sec. S1). Inelastic neutron-scattering data were collected on the SEQUOIA instrument [32,33] at the Spallation Neutron Source, Oak Ridge National Laboratory (USA). Incoming neutron energies of $E_i = 40$ and 80 meV were used, yielding elastic energy resolutions of 0.8(4) and 1.6(8) meV, respectively. The sample was mounted with the [100] and [010] directions in the horizontal scattering plane, cooled to $T = 20$ K using a closed-cycle refrigerator, and rotated about a vertical axis in steps of 1° over a range $> 90°$. The data were converted to absolute units in MANTID [34] using measurements of a vanadium standard, analyzed in HORACE [35] where background contributions and Bragg peaks from the sample were masked, and symmetrized in the $m\bar{3}m$ Laue class (see Sec. S2 [31]). The normalized magnetic intensity can be written $I(\mathbf{Q}, E) = (\frac{1}{2}\gamma r_0)^2[gf(|\mathbf{Q}|)]^2\mathcal{S}(\mathbf{Q}, E)$, where $(\frac{1}{2}\gamma r_0)^2 = 0.072\,65 \times 10^{-24}$ cm^2 [36], $f(|\mathbf{Q}|)$ is the Cr^{3+} magnetic form factor, and $\mathcal{S}(\mathbf{Q}, E)$ is the magnetic scattering function. We obtained energy-integrated quantities $I_\alpha(\mathbf{Q}) \equiv \int_0^{E'} dE E^\alpha (1 + e^{-E/k_B T})\mathcal{S}(\mathbf{Q}, E)$, where $\alpha \in \{0, 1\}$, and $E' = 20$ meV is chosen to encompass the magnetic excitation bandwidth. The quantities $I_0(\mathbf{Q})$ and $I_1(\mathbf{Q})$ are proportional to the instantaneous magnetic structure factor $\mathcal{S}(\mathbf{Q})$ and the first moment $\mathcal{K}(\mathbf{Q})$, respectively, with the constant of proportionality $F(|\mathbf{Q}|) = (\frac{1}{2}\gamma r_0)^2[gf(|\mathbf{Q}|)]^2$.

To model the magnetism of $MgCr_2O_4$, we use the Heisenberg model $\mathcal{H} = \frac{1}{2}\sum_{ij} J_{ij}\mathbf{S}_i \cdot \mathbf{S}_j$, where $\mathbf{S}_i$ represents the spin at one of the N sites $\mathbf{R}_i$ of the pyrochlore lattice, and the four interactions $J_{ij} \in \{J_1, J_2, J_{3a}, J_{3b}\}$ extend to third-nearest neighbors [Fig. 1(a)]. We will show that it is crucial to model the two inequivalent third-neighbor pathways J_{3a} and J_{3b} separately. Our choice of a Heisenberg model is motivated by the small orbital contribution to the magnetic moment ($g \approx 2.05$) and the electron spin resonance results above T_N [37,38]. This is verified by a preliminary reverse Monte Carlo analysis [39–42] that reveals an isotropic distribution of spin orientations (see Sec. S3 [31]). For a Heisenberg paramagnet, the structure factor is the Fourier transformation of instantaneous two-spin correlators, $\mathcal{S}(\mathbf{Q}) = (2/3N)\sum_{ij}\langle \mathbf{S}_i \cdot \mathbf{S}_j\rangle \cos(\mathbf{Q}\cdot\mathbf{r}_{ij})$, where $\mathbf{r}_{ij} = \mathbf{R}_i - \mathbf{R}_j$ is the vector between the spin pair. The first moment contains correlators weighted by the corresponding interactions [43,44], $\mathcal{K}(\mathbf{Q}) = -(1/3N)\sum_{ij} J_{ij}\langle \mathbf{S}_i \cdot \mathbf{S}_j\rangle [1 - \cos(\mathbf{Q}\cdot\mathbf{r}_{ij})]$. As J_{3a} and J_{3b} are symmetry inequivalent but associated with the same lattice harmonics, it is impossible to determine their values by a simple ratio between Fourier coefficients of the structure factor and the first moment. Therefore, we employ the self-consistent Gaussian approximation (SCGA) [45] to calculate $\mathcal{S}(\mathbf{Q})$ and $\mathcal{K}(\mathbf{Q})$ from the magnetic interaction matrix; this method is in excellent quantitative agreement with classical Monte Carlo simulations (see Sec. S5 [31]).

Determining the magnetic interactions of $MgCr_2O_4$ is a challenging problem, because the spin correlations of the model are essentially degenerate along the line $J_2 = J_{3a}$ in the interaction space [46]. Consequently, we used three complementary approaches. First, we performed a global fit to $\mathcal{S}(\mathbf{Q})$ and $\mathcal{K}(\mathbf{Q})$ for a grid of values of J_2 and J_{3a}, with J_1 and J_{3b} fitted at each grid point. The corresponding goodness-of-fit χ^2, shown in Fig. 1(b), reveals a shallow valley of possible minima (see Sec. S4 [31]). Second, we calculated the goodness-of-fit to the temperature dependence of bulk magnetic susceptibility data between 20 K and 400 K for all the parameter sets $\{J_1, J_2, J_{3a}, J_{3b}\}$ extracted from the $\mathcal{S}(\mathbf{Q}) + \mathcal{K}(\mathbf{Q})$ fits. The intersection of χ^2 minima for these two results yields $J_1 = 38.05(3)$ K, $J_2/J_1 = 0.0815$, $J_{3a}/J_1 = 0.1050$, and $J_{3b}/J_1 = 0.0085(1)$ [red star in Fig. 1(b)]. Finally, we validated these parameters using fits to the energy-resolved $S(\mathbf{Q}, \omega)$, as discussed below [Fig. 2].

In Fig. 1, we compare the experimental $I_\alpha(\mathbf{Q})$ with SCGA calculations for our optimized exchange parameters. The FN interactions are small, with a maximum of $J_{3a} \approx 0.1J_1$, and all of them are antiferromagnetic, in contrast to first-principles estimates [47]. Crucially, however, these interactions quantitatively explain the clusterlike scattering [13,15,17,23] [Fig. 1(d)–1(e)]. Compared to the NN model, our model correctly captures the suppressed intensity at the (2,0,0) and (2,2,0) pinch-point positions [Fig. 1(c)], indicating the destruction of the Coulomb phase by FN interactions [45]. In real space, the spin correlators as a function of distance show an alternation in sign, which explains the apparent success of the decoupled hexagonal spin-cluster model (see Sec. S5 [31]). However, our FN Heisenberg model enables three key advances. First, it allows a complete microscopic description of the spin dynamics. Second, it allows the frustration to be understood in terms of the degeneracies of the model, and third, it enables the nature of the low-temperature ordered phases to be predicted in the absence of magnetoelastic effects. We discuss these results in turn below.

Magnetic excitation spectra of our sample are presented in Fig. 2. The excitations are gapless with a bandwidth of $\approx$20 meV ($\sim 4J_1S$), although the dominant contribution to the spectral weight resides below $\approx$5 meV ($\sim J_1S$) [Fig. 2(a)]. Close to the suppressed pinch point at

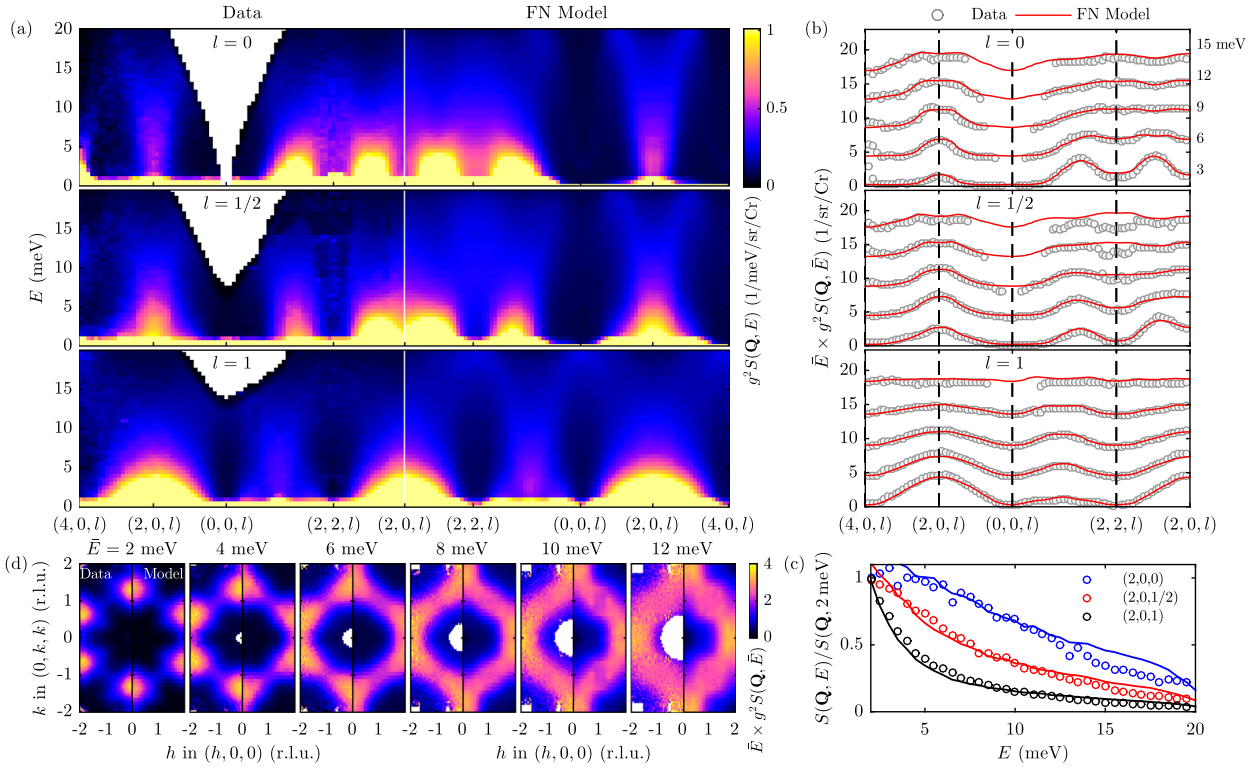

FIG. 2. Magnetic excitation spectra of $MgCr_2O_4$ at $T = 20$ K measured with incident neutron energy $E_i = 40$ meV, and comparison with linear spin-wave theory (LSWT) calculations for our FN model. (a) Momentum-energy slices through $g^2S(\mathbf{Q}, E)$ along different paths, comparing data (left column) and FN model (right column). (b) Cuts at constant energies $\bar{E} \pm 0.2$ meV through the data (gray circles) and FN model (red lines), where $\bar{E}$ is labeled on each plot. The intensity is multiplied by $\bar{E}$ and offset by 4 $\text{sr}^{-1}\,\text{Cr}^{-1}$ for clarity. (c) Energy dependence of the experimental (colored circles) and modeled (colored lines) dynamical structure factor at selected momenta, normalized to the energy transfer $E_0 = 2$ meV. (d) Slices at constant energies $\bar{E} \pm 0.2$ meV through the data (left column) and the FN model (right column) in the (h, k, k) plane. Throughout, blank space is due to kinematic constraints on the scattering, and the extra intensity at (4,0,0) arises from a strong nuclear Bragg peak and its associated acoustic phonon.

(2,0,0), excitations are relatively sharp and dispersive along the $(\xi, 0, 0)$ direction [Fig. 2(b)], a feature also observed in $NaCaNi_2F_7$ [11]. Along other directions, such as $(2, \xi, 0)$ and $(\xi, \xi, 0)$, the excitations form a broad continuum [Fig. 2(a)] whose energy dependence is Lorentzian with a $\mathbf{Q}$-dependent relaxation rate [Fig. 2(c)]. A simple factorization of the dynamic response as $\mathcal{S}(\mathbf{Q}, E) = \mathcal{S}(\mathbf{Q})f(E)$, which implies spatially incoherent excitations, is not possible for $MgCr_2O_4$ [Fig. 2(d)], in contrast to theoretical predictions for the lowest branch of excitations in the NN model [48].

To examine the nature of excitations, we calculated $\mathcal{S}(\mathbf{Q}, E)$ in the paramagnetic regime using linear spin-wave theory (LSWT) in a framework previously used to model metallic spin glasses [49,50]. For a given set of interactions, we use Monte Carlo simulations to generate ensembles of spin configurations at low but finite temperature to avoid ordering, calculate harmonic fluctuations of each spin configuration, and average $\mathcal{S}(\mathbf{Q}, E)$ over these samples (see Sec. S6 [31]). We compared LSWT calculations—performed for several sets of interactions near the shallow χ^2 minimum of Fig. 1(b)—with the entire 4D momentum-energy dependence of our experimental data (see Sec. S7 [31]). The best match is obtained for our previously-determined FN model, with LSWT calculations in striking agreement with the experimental observations [Fig. 2].

Our microscopic model also explains the persistence of a classical spin liquid in $MgCr_2O_4$ despite FN interactions. In classical spin liquids, the lowest-energy eigenvalues of the interaction matrix are degenerate throughout large regions of the Brillouin zone, which suppresses magnetic ordering. We find that for the FN parameters of $MgCr_2O_4$, ordering wave vectors $\boldsymbol{\kappa}$ with energies within 0.5% of the global energy minimum describe a large surface near the zone boundary [Fig. 3(a)]. This result is surprising because FN interactions are generically expected to lift the degeneracy of the NN model. To explain it, we calculated the phase diagram of ordered states as a function of J_2, J_{3a}, and J_{3b} [Fig. 3(b)]. Crucially, we uncover planes in interaction space along which the degeneracy of possible ordered states is exact and macroscopic. Our FN parameters place $MgCr_2O_4$ in proximity to such a phase, for which wave vectors of the type $\boldsymbol{\kappa} = (1, h, 0)$ are degenerate [blue lines

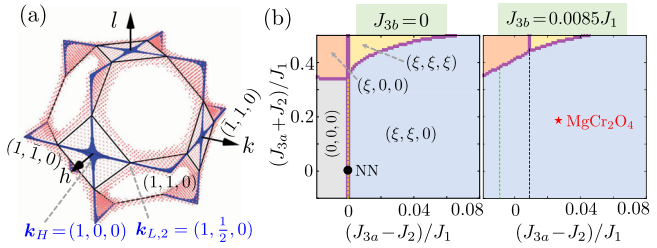

FIG. 3. (a) Sets of ordering wave vectors $\boldsymbol{\kappa}$ with nearly-degenerate energies represented in the Brillouin zone as colored surfaces. The pink surface shows wave vectors with energies within ~0.5% of the global energy minimum for the FN interaction parameters of $MgCr_2O_4$. The blue lines show wave vectors with energy equal to the global energy minimum for the macroscopically-degenerate phases represented by a blue dashed line in the phase diagram. (b) Mean-field phase diagrams of our FN Heisenberg model as a function of J_2 and J_{3a}, showing results for $J_{3b} = 0$ (left) and $J_{3b} = 0.0085 J_1$ (right). Phases with different ordering wave vectors $\boldsymbol{\kappa}$ are shown in different colors. Special phases (dashed lines) correspond to a macroscopic number of ordering wave vectors with degenerate energies. They emerge from $J_{3a} - J_2 = 0$ (yellow line), which corresponds to the NN model, to form two half-planes corresponding to $J_{3a} - J_2 = \mp J_{3b}$ (green and blue lines).

in Fig. 3(a)]. The corresponding states are a degenerate set of coplanar spirals (see Sec. S8 [31]), analogous to the "spiral spin liquid" states previously known only for the $J_1 - J_2$ model on the diamond lattice [51]. This result explains the similarity of clusterlike scattering in $MgCr_2O_4$ to neutron-scattering data for diamond-lattice systems such as $MnSc_2S_4$ [52].

Our analysis sets a benchmark for the comprehensive determination of magnetic interactions in materials where the traditional approach of spin-wave dispersion modeling is not available—either because the system does not order at an accessible temperature, or because the nature of this ordering is controlled by a magnetic Hamiltonian that is distinct from that of the paramagnetic phase due to magnetoelastic effects. The latter is the case in frustrated spinels such as $MgCr_2O_4$ and $ZnCr_2O_4$. Below T_N, the presence of several symmetry-unrelated ordering wave vectors makes magnetic structure solution very challenging. However, our results present a key insight: the degeneracy of our spiral spin liquid state encompasses two of the ordering wave vectors, $\boldsymbol{\kappa}_H$ and $\boldsymbol{\kappa}_{L,2}$, that are observed experimentally below T_N in $MgCr_2O_4$ and $ZnCr_2O_4$. This result suggests that the complex magnetic ordering observed in these frustrated spinels is a consequence of the near degeneracy of competing ordered states shown in Fig. 3(a). While the exact ground state is likely selected by magnetostructural effects beyond the Heisenberg model, we anticipate that our paramagnetic Hamiltonian will provide a valuable starting point to develop a microscopic theory of magnetic ordering in these complex materials. It is remarkable that, within the resolution of our experiment, the spin dynamics of $MgCr_2O_4$ at $T = 20$ K can be entirely described by spins precessing around their local mean field, with no evidence of quantum effects [11]. Crucially, this excludes fractionalization and short lifetime as the physical origin for the broad momentum-energy response; rather, it indicates that scattering is broad in the wave vector because excitations propagate in a spatially disordered background. Similar observations for $NaCaNi_2F_7$ [53], a pyrochlore antiferromagnet with a range of interactions and a spin quantum number that differs from $MgCrO_4$, suggest the robustness of our theoretical results.

We thank Oleg Tchernyshyov for many useful discussions during the earlier stages of this project. The work at Georgia Tech and at the Institute for Quantum Matter was supported by the U.S. Department of Energy, Office of Basic Energy Sciences, Materials Sciences and Engineering Division under Awards No. DE-SC-0018660 and No. DE-FG02-08ER46544, respectively. The work at Oxford University was supported by the EPSRC under Grant No. EP/I032487/1. The research at Oak Ridge National Laboratory's Spallation Neutron Source was sponsored by the U.S. Department of Energy, Office of Basic Energy Sciences, Scientific User Facilities Division. J. A. M. P. acknowledges financial support from Churchill College, Cambridge (UK). C. B. was supported by the Gordon and Betty Moore foundation under GBMF 4532. M. M. and J. T. C. acknowledge the Kavli Institute for Theoretical Physics (KITP) where part of this research was started. KITP is supported by the National Science Foundation under Grant No. NSF-PHY-1748958.

*Present address: Stanford Institute for Materials and Energy Sciences, SLAC National Accelerator Laboratory, Menlo Park, CA 94025, USA.
†Present address: Cavendish Laboratory, Department of Physics, University of Cambridge, JJ Thomson Ave., Cambridge CB3 0HE, UK.
‡mourigal@gatech.edu

[1] P. W. Anderson, Phys. Rev. **102**, 1008 (1956).
[2] J. Villain, Z. Phys. B **33**, 31 (1979).
[3] J. N. Reimers, Phys. Rev. B **45**, 7287 (1992).
[4] R. Moessner and J. T. Chalker, Phys. Rev. Lett. **80**, 2929 (1998).
[5] C. L. Henley, Annu. Rev. Condens. Matter Phys. **1**, 179 (2010).
[6] S. T. Bramwell and M. J. Gingras, Science **294**, 1495 (2001).
[7] T. Fennell, P. P. Deen, A. R. Wildes, K. Schmalzl, D. Prabhakaran, A. T. Boothroyd, R. J. Aldus, D. F. McMorrow, and S. T. Bramwell, Science **326**, 415 (2009).
[8] D. J. P. Morris, D. A. Tennant, S. A. Grigera, B. Klemke, C. Castelnovo, R. Moessner, C. Czternasty, M. Meissner, K. C. Rule, J.-U. Hoffmann, K. Kiefer, S. Gerischer, D. Slobinsky, and R. S. Perry, Science **326**, 411 (2009).

[9] J. W. Krizan and R. J. Cava, Phys. Rev. B **89**, 214401 (2014).
[10] K. A. Ross, J. W. Krizan, J. A. Rodriguez-Rivera, R. J. Cava, and C. L. Broholm, Phys. Rev. B **93**, 014433 (2016).
[11] K. W. Plumb, H. J. Changlani, A. Scheie, S. Zhang, J. W. Krizan, J. A. Rodriguez-Rivera, Y. Qiu, B. Winn, R. J. Cava, and C. L. Broholm, Nat. Phys. **15**, 54 (2019).
[12] J. H. Chung, M. Matsuda, S. H. Lee, K. Kakurai, H. Ueda, T. J. Sato, H. Takagi, K. P. Hong, and S. Park, Phys. Rev. Lett. **95**, 247204 (2005).
[13] S. H. Lee, C. Broholm, W. Ratcliff, G. Gasparovic, Q. Huang, T. H. Kim, and S. W. Cheong, Nature (London) **418**, 856 (2002).
[14] H. Suzuki and Y. Tsunoda, J. Phys. Chem. Solids **68**, 2060 (2007).
[15] K. Tomiyasu, H. Suzuki, M. Toki, S. Itoh, M. Matsuura, N. Aso, and K. Yamada, Phys. Rev. Lett. **101**, 177401 (2008).
[16] O. Tchernyshyov, R. Moessner, and S. L. Sondhi, Phys. Rev. Lett. **88**, 067203 (2002).
[17] K. Tomiyasu, T. Yokobori, Y. Kousaka, R. I. Bewley, T. Guidi, T. Watanabe, J. Akimitsu, and K. Yamada, Phys. Rev. Lett. **110**, 077205 (2013).
[18] G. Blasse and J. Fast, Philips Res. Rep. **18**, 393 (1963).
[19] T. Rudolf, C. Kant, F. Mayr, J. Hemberger, V. Tsurkan, and A. Loidl, New J. Phys. **9**, 76 (2007).
[20] S. E. Dutton, Q. Huang, O. Tchernyshyov, C. L. Broholm, and R. J. Cava, Phys. Rev. B **83**, 064407 (2011).
[21] S. Koohpayeh, J.-J. Wen, M. Mourigal, S. Dutton, R. Cava, C. Broholm, and T. McQueen, J. Cryst. Growth **384**, 39 (2013).
[22] R. Moessner and A. J. Berlinsky, Phys. Rev. Lett. **83**, 3293 (1999).
[23] S. Gao *et al.*, Phys. Rev. B **97**, 134430 (2018).
[24] S. Klemme, H. S. C. O'Neill, W. Schnelle, and E. Gmelin, Am. Mineral. **85**, 1686 (2000).
[25] H. Ehrenberg, M. Knapp, C. Baehtz, and S. Klemme, Powder Diffr. **17**, 230 (2002).
[26] L. Ortega-San-Martín, A. J. Williams, C. D. Gordon, S. Klemme, and J. P. Attfield, J. Phys. Condens. Matter **20**, 104238 (2008).
[27] M. C. Kemei, P. T. Barton, S. L. Moffitt, M. W. Gaultois, J. A. Kurzman, R. Seshadri, M. R. Suchomel, and Y.-I. Kim, J. Phys. Condens. Matter **25**, 326001 (2013).
[28] H. J. Xiang, E. J. Kan, S.-H. Wei, M.-H. Whangbo, and X. G. Gong, Phys. Rev. B **84**, 224429 (2011).
[29] G. J. Nilsen, Y. Okamoto, T. Masuda, J. Rodriguez-Carvajal, H. Mutka, T. Hansen, and Z. Hiroi, Phys. Rev. B **91**, 174435 (2015).
[30] H. Shaked, J. M. Hastings, and L. M. Corliss, Phys. Rev. B **1**, 3116 (1970).
[31] See Supplemental Material at http://link.aps.org/supplemental/10.1103/PhysRevLett.122.097201 for further details on our analysis.
[32] G. E. Granroth, A. I. Kolesnikov, T. E. Sherline, J. P. Clancy, K. A. Ross, J. P. C. Ruff, B. D. Gaulin, and S. E. Nagler, J. Phys. Conf. Ser. **251**, 012058 (2010).
[33] M. B. Stone, J. L. Niedziela, D. L. Abernathy, L. DeBeer-Schmitt, G. Ehlers, O. Garlea, G. E. Granroth, M. Graves-Brook, A. I. Kolesnikov, A. Podlesnyak, and B. Winn, Rev. Sci. Instrum. **85**, 045113 (2014).
[34] O. Arnold, J.-C. Bilheux, J. Borreguero, A. Buts, S. I. Campbell, L. Chapon, M. Doucet, N. Draper, R. F. Leal, M. Gigg *et al.*, Nucl. Instrum. Methods Phys. Res., Sect. A **764**, 156 (2014).
[35] R. Ewings, A. Buts, M. Le, J. van Duijn, I. Bustinduy, and T. Perring, Nucl. Instrum. Methods Phys. Res., Sect. A **834**, 132 (2016).
[36] G. Xu, Z. Xu, and J. M. Tranquada, Rev. Sci. Instrum. **84**, 083906 (2013).
[37] C. Blanchard, A. Deville, A. Boukenter, B. Champagnon, and E. Duval, J. Phys. (Paris) **47**, 1931 (1986).
[38] M. Yoshida, T. Hirano, Y. Inagaki, S. Okubo, H. Ohta, H. Kikuchi, I. Kagomiya, M. Toki, and K. Kohn, J. Phys. Soc. Jpn. **75**, 044709 (2006).
[39] R. L. McGreevy and L. Pusztai, Mol. Simul. **1**, 359 (1988).
[40] J. A. M. Paddison and A. L. Goodwin, Phys. Rev. Lett. **108**, 017204 (2012).
[41] J. A. M. Paddison, G. Ehlers, O. A. Petrenko, A. R. Wildes, J. S. Gardner, and J. R. Stewart, J. Phys. Condens. Matter **29**, 144001 (2017).
[42] J. A. M. Paddison, M. J. Gutmann, J. R. Stewart, M. G. Tucker, M. T. Dove, D. A. Keen, and A. L. Goodwin, Phys. Rev. B **97**, 014429 (2018).
[43] P. C. Hohenberg and W. F. Brinkman, Phys. Rev. B **10**, 128 (1974).
[44] M. B. Stone, I. Zaliznyak, D. H. Reich, and C. Broholm, Phys. Rev. B **64**, 144405 (2001).
[45] P. H. Conlon and J. T. Chalker, Phys. Rev. B **81**, 224413 (2010).
[46] G.-W. Chern, R. Moessner, and O. Tchernyshyov, Phys. Rev. B **78**, 144418 (2008).
[47] A. N. Yaresko, Phys. Rev. B **77**, 115106 (2008).
[48] P. H. Conlon and J. T. Chalker, Phys. Rev. Lett. **102**, 237206 (2009).
[49] L. R. Walker and R. E. Walstedt, Phys. Rev. Lett. **38**, 514 (1977).
[50] L. R. Walker and R. E. Walstedt, Phys. Rev. B **22**, 3816 (1980).
[51] D. Bergman, J. Alicea, E. Gull, S. Trebst, and L. Balents, Nat. Phys. **3**, 487 (2007).
[52] S. Gao, O. Zaharko, V. Tsurkan, Y. Su, J. S. White, G. Tucker, B. Roessli, F. Bourdarot, R. Sibille, D. Chernyshov, T. Fennell, A. Loidl, and C. Rüegg, Nat. Phys. **13**, 157 (2017).
[53] S. Zhang, H. J. Changlani, K. W. Plumb, O. Tchernyshyov, and R. Moessner, arXiv:1810.09481.